MOLECULAR AND CELLULAR BIOLOGY, Feb. 2002, p. 1233–1245 Vol. 22, No. 4
0270-7306/02/$04.00+0 DOI: 10.1128/MCB.22.4.1233–1245.2002

Developmental Defects and Male Sterility in Mice Lacking the Ubiquitin-Like DNA Repair Gene *mHR23B*

Jessica M. Y. Ng,[1] Harry Vrieling,[2] Kaoru Sugasawa,[3,4] Marja P. Ooms,[5] J. Anton Grootegoed,[5] Jan T. M. Vreeburg,[5] Pim Visser,[1] Rudolph B. Beems,[6] Theo G. M. F. Gorgels,[7] Fumio Hanaoka,[3,4,8] Jan H. J. Hoeijmakers,[1]* and Gijsbertus T. J. van der Horst[1]

MGC-Department of Cell Biology and Genetics, Centre for Biomedical Genetics,[1] and Department of Endocrinology and Reproduction,[5] Erasmus University Rotterdam, Rotterdam, MGC-Department of Radiation Genetics and Chemical Mutagenesis, Leiden University Medical Center, 2333 AL Leiden,[2] National Institute of Public Health and the Environment, 3720 BA Bilthoven,[6] The Netherlands Ophthalmic Research Institute-KNAW, 1105 BA Amsterdam,[7] The Netherlands, and Cellular Physiology Laboratory, RIKEN (The Institute of Physical and Chemical Research),[3] and Core Research for Evolutional Science and Technology, Japan Science and Technology Corporation,[4] Wako, Saitama 351-0198, and Institute for Molecular and Cellular Biology, Osaka University, Suita, Osaka 565-0871,[8] Japan

Received 23 August 2001/Returned for modification 27 September 2001/Accepted 29 October 2001

***mHR23B* encodes one of the two mammalian homologs of *Saccharomyces cerevisiae* RAD23, a ubiquitin-like fusion protein involved in nucleotide excision repair (NER). Part of mHR23B is complexed with the XPC protein, and this heterodimer functions as the main damage detector and initiator of global genome NER. While *XPC* defects exist in humans and mice, mutations for *mHR23A* and *mHR23B* are not known. Here, we present a mouse model for *mHR23B*. Unlike *XPC*-deficient cells, *mHR23B*$^{-/-}$ mouse embryonic fibroblasts are not UV sensitive and retain the repair characteristics of wild-type cells. In agreement with the results of in vitro repair studies, this indicates that mHR23A can functionally replace mHR23B in NER. Unexpectedly, *mHR23B*$^{-/-}$ mice show impaired embryonic development and a high rate (90%) of intrauterine or neonatal death. Surviving animals display a variety of abnormalities, including retarded growth, facial dysmorphology, and male sterility. Such abnormalities are not observed in *XPC* and other NER-deficient mouse mutants and point to a separate function of mHR23B in development. This function may involve regulation of protein stability via the ubiquitin/proteasome pathway and is not or only in part compensated for by mHR23A.**

Nucleotide excision repair (NER) is the major repair system for the removal of DNA lesions induced by UV light and numerous chemical agents (12, 49). The cut-and-patch-type reaction mechanism involves the concerted action of more than 25 proteins, sequentially implicated in recognition of DNA damage, unwinding of the DNA around the lesion, excision of a single-stranded piece of DNA containing the damage, and subsequent gap filling DNA synthesis and ligation (10). NER consists of two subpathways. Genome-wide repair is taken care of by the global genome NER (GG-NER) process, acting irrespective of the genomic location of the lesion or cell cycle stage. However, some lesions (e.g., UV-induced cyclobutane pyrimidine dimers) are repaired less efficiently by GG-NER. To prevent such lesions from obstructing the vital process of transcription for too long, the transcription-coupled NER (TC-NER) subpathway acts as a fast backup system for clearing the template strands of actively transcribed genes (16, 17).

Defective NER is associated with three clinically and genetically heterogeneous human syndromes: xeroderma pigmentosum (XP), Cockayne syndrome (CS), and trichothiodystrophy (TTD) (3). Patients suffering from XP (complementation groups XP-A to XP-G) exhibit severe sensitivity to sunlight (UV), ocular symptoms, and cutaneous abnormalities, including a very strong predisposition to develop skin cancer. Most XP patients carry defects in GG-NER and TC-NER, but only the GG-NER pathway is affected in XP-C patients (43–45).

The XPC protein is essential for GG-NER of various types of DNA damage and is found in a tight complex with hHR23B, one of the two human homologs of the *Saccharomyces cerevisiae* DNA repair protein RAD23 (26). hHR23B stimulates the repair activity of XPC in in vitro reconstitution assays with recombinant proteins (37). A 56-amino-acid segment with a predicted helical amphipathic structure containing the XPC-binding domain of hHR23B appears sufficient for XPC stimulation. This suggests that hHR23B has a structural rather than catalytic function (25). A vast majority of XPC protein is bound to hHR23B in vivo. However, in vitro, hHR23A, the second human homolog of RAD23, can substitute for hHR23B in binding and stimulating XPC. This opens the possibility that both proteins are functionally interchangeable to some extent (39, 41). The XPC-hHR23B complex has been identified as the primary DNA damage sensor that initiates GG-NER and has been shown to interact directly with the essential repair and transcription factor TFIIH in vivo and in vitro (38, 50). The XPC-hHR23B complex senses different types of damage based on disrupted base pairing and stimulates the association of TFIIH with damaged DNA in cell extracts (50). After the

* Corresponding author. Mailing address: MGC-Department of Cell Biology and Genetics, CBG, Erasmus University Rotterdam, P.O. Box 1738, Rotterdam, The Netherlands. Phone: 31-10-4087199. Fax: 31-10-4089468. E-mail: hoeijmakers@gen.fgg.eur.nl.

initial subpathway-specific lesion detection, the XPB and XPD helicase subunits of TFIIH open the DNA helix around the lesion. XPA together with the heterotrimeric replication protein A may function as a common damage verifier before the DNA is incised on both sides of the injury by the XPG and ERCC1/XPF endonucleases (10, 50).

In addition to the XPC-binding domain, *S. cerevisiae* and mammalian RAD23 proteins harbor an amino-terminal ubiquitin-like (UbL) moiety and two so-called ubiquitin-associated (UBA) domains (21, 25). In *S. cerevisiae*, the UbL domain is indispensable for the repair function of RAD23 (28, 48). Moreover, hHR23A and hHR23B interact with the S5a subunit of the 26S proteasome, and hHR23A serves as a substrate for E6-associated protein-mediated ubiquitination (20, 23). These findings strongly suggest that the RAD23 homologs are involved in the ubiquitin/proteasome pathway.

Although hHR23A can functionally replace hHR23B in vitro during NER, it is unknown whether and to which extent these two human RAD23 homologs can substitute for each other in vivo. Moreover, while for most other NER genes, natural and/or laboratory-made human and rodent mutant cell lines are available, *HR23*-deficient cell lines have not been described. Thus, to address the biological relevance of mammalian RAD23 homologs and their relationship to XPC in NER, we have inactivated the mouse homolog of HR23B *(mHR23B)* by gene targeting. In the present paper, we describe the phenotypes of *mHR23B*-deficient mice and cells.

MATERIALS AND METHODS

Construction of *mHR23B* targeting vector. Isogenic mouse genomic DNA was isolated from an Ola129-derived phage lambda library after probing with human *HR23B* cDNA sequences. A 13.6-kb *Sal*I fragment, containing three exons (exons II to IV), was subcloned into the *Sal*I site of a pUC vector, designated pMHR23B1 (16.5 kbp). Following several subcloning steps, a 2.5-kb *Eco*RI fragment (containing exon II) was cloned at the *Cla*I site and a 4.5-kb *Nco*I-*Sac*I fragment (containing exon IV) was positioned between the *Not*I-*Sac*II sites of the targeting vector pMHR23B-UMS-E3 (6.9 kb) representing the 5′ and 3′ arms of homology, respectively. Thus, in the targeting vector, exon III (amino acids 148 to 228) was replaced with a cassette containing (*PGK* promoter-driven) neomycin resistance gene and an upstream mouse sequence (described as a transcriptional stop sequence [19]). The vector also contained the negative selectable marker HSV-TK (herpes simplex virus thymidine kinase gene).

ES cell culture and transfection. The Ola129-derived embryonic stem (ES) cell line E14 was electroporated with the *mHR23B* targeting construct and cultured on dishes treated with gelatin as described previously (40). G418 (Geneticin; Gibco) was added 24 h after electroporation to a final concentration of 200 μg/ml, and the cells were maintained under selection for 6 to 8 days. Genomic DNA from individual G418-resistant clones was digested with *Sac*I and analyzed by Southern blotting using a genomic PCR fragment (255 bp), isolated between *Sac*I-*Eco*RI sites (upstream of exon II), as a probe. Targeted clones, with the correct hybridizing *Sac*I fragments, were subsequently screened with a fragment of the neomycin resistance gene as a probe to confirm proper homologous recombination.

Generation of the *mHR23B*-deficient mice and fibroblasts. Cells of *mHR23B*-targeted clones were karyotyped, and ES cells from two independent clones with 40 chromosomes were injected into 3.5-day-old blastocysts isolated from pregnant C57BL/6 female mice (40). Male chimeric mice were mated with C57BL/6 females to obtain heterozygote animals. Germ line transmission was observed in the coat color of the F_1 offspring. Heterozygous male and female mice were interbred to generate $mHR23B^{+/+}$, $mHR23B^{+/-}$, and $mHR23B^{-/-}$ mice. Genotyping was performed by Southern blotting with genomic DNA prepared from tail biopsies of 10- to 14-day-old pups.

Primary mouse embryonic fibroblasts (MEFs) (at least three independent lines per genotype) were isolated from day 13.5 embryos obtained from matings between $mHR23B^{+/-}$ mice (F_1). Part of the embryo was used for genotyping. The remaining embryonic tissue was minced using a pair of scissors and immersed in a thin layer of culture medium (Dulbecco modified Eagle medium with 10% fetal calf serum [Gibco BRL]) supplemented with 15% fetal calf serum, 2 mM glutamate, 50 μg of penicillin per ml, and 50 μg of streptomycin per ml.

Northern blot analysis. Total RNA samples (20 μg) were separated on 0.9% agarose gel and transferred to Hybond-N+ membrane (Amersham Pharmacia Biotech). Total RNA was isolated from *mHR23B* MEFs using the acid guanidinium-phenol-chloroform (AGPC) method described previously (5). RNA blots were hybridized using ^{32}P-labeled *mHR23A* and *mHR23B* cDNA probes.

Protein analysis. Immunoblot analysis of mHR23B protein was performed on fibroblast extracts obtained by sonification (5×10^6 cells in 300 μl of phosphate-buffered saline containing phenylmethylsulfonyl fluoride and CLAP [chymostatin, leupeptin, antipain, and pepstatin A]). Eighty micrograms of total cellular protein per lane was separated on sodium dodecyl sulfate–8% polyacrylamide gels, blotted to nitrocellulose filters (Schleicher & Schuell), and probed with rabbit polyclonal antibodies recognizing mHR23B. Bands were visualized using peroxidase-conjugated secondary antibodies.

DNA repair assays. UV sensitivity was determined as described previously (36). MEF cultures were exposed to different doses of UV-C (254-nm-wavelength light; Philips TUV lamp) and allowed to grow for another 3 to 5 days before reaching confluence. The number of proliferating cells was estimated by scintillation counting of the radioactivity incorporated during a 3-h pulse with [^{3}H]thymidine (5 μCi/ml; specific activity [SA], 40 to 60 Ci/mmol; Amersham). Cell survival was expressed as the ratio of ^{3}H incorporated in irradiated cells to ^{3}H incorporated in nonirradiated cells.

UV-induced global genome repair was assayed using the unscheduled DNA synthesis (UDS) method described previously (47). In short, cells grown on coverslips were exposed to 254-nm-wavelength UV light (16 J/m^2) and labeled with [*methyl*-^{3}H]thymidine (10 μCi/ml; SA, 40 to 60 Ci/mmol). Repair capacity was quantified by counting grains after autoradiography.

RNA synthesis recovery after UV irradiation (27) was measured as follows. Cells were labeled with [2-^{14}C]thymidine (0.05 μCi/ml; SA, 56 Ci/mmol) for 24 h, exposed to different doses of 254-nm-wavelength UV light, allowed to recover for 16 h, labeled with [5,6-^{3}H]uridine (10 μCi/ml; SA, 47 Ci/mmol) for 1 h, and processed for scintillation counting. The relative rate of RNA synthesis was expressed as the ratio of radioactivity in UV-irradiated cells to that in nonirradiated cells. Comparable results were also obtained by counting grains after autoradiography. The relative rate of RNA synthesis was expressed as the number of autoradiographic grains over the UV-exposed nuclei divided by the number of grains over the nuclei of nonirradiated cells on parallel slides (data not shown).

Histology and electron microscopical analysis. For histological examination, dissected tissues fixed in Bouin or in 10% neutral buffered formalin were processed and embedded in paraffin. Mounted sections (5 to 8 μm thick) were stained with hematoxylin and eosin using routine procedures.

For transmission electron microscopy, small pieces of tissue were fixed in buffered 4% paraformaldehyde and postfixed in 1% OsO_4 plus $K_3Fe(CN)_6$ (9). After the tissue samples were dehydrated and embedded in Epon, 1-μm-thick sections were cut and stained with methylene blue.

RESULTS

Targeted disruption of the mouse *mHR23B* gene. The mouse *mHR23B* locus was isolated and partly characterized. Deletion of exon III not only removes the sequence encoding amino acid residues 148 to 228 of the mHR23B protein but also results in a frameshift and accordingly is expected to give rise to a null allele (Fig. 1A). Following transfection of ES cell line E14, properly targeted heterozygous ES cells were obtained at a frequency of 21% (Fig. 1B). Two independent ES clones for which the absence of visible chromosomal abnormalities and additional randomly integrated constructs had been verified (data not shown) were used for blastocyst injections. Germ line transmission was obtained for both clones. Heterozygous offspring from matings between chimeric males and C57BL/6 female mice were intercrossed in order to generate homozygous mutant *mHR23B* animals (Fig. 1C). In parallel, these matings served to isolate MEFs of different genotypes from day 13.5 embryos. The effect of targeted disruption on the

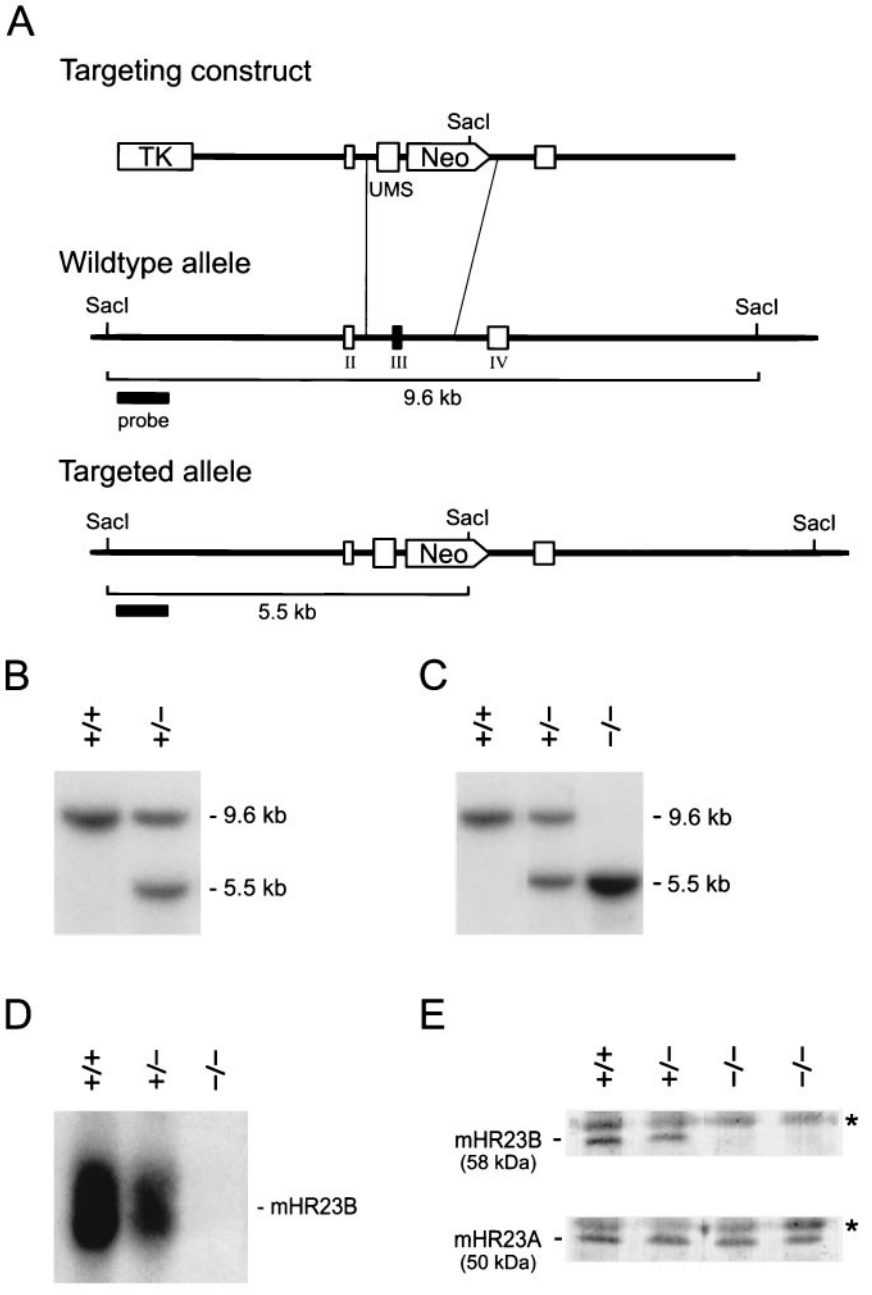

FIG. 1. Targeted disruption of the *mHR23B* gene by homologous recombination. (A) Genomic organization and disruption strategy for *mHR23B* showing the gene, the targeting construct, and the targeted *mHR23B* allele. Exon III is deleted, and the upstream mouse sequence and Neo cassettes are inserted between exon II and exon IV. (B) Southern blot analysis of *Sac*I-digested DNA from ES cells showing the 9.6-kb and 5.5-kb fragments representing the wild-type and targeted alleles of *mHR23B,* respectively. (C) Southern blot analysis of *Sac*I-digested tail DNA from $mHR23B^{+/+}$, $mHR23B^{+/-}$, and $mHR23B^{-/-}$ mice. (D) RNA blot analysis of *mHR23B* mRNA in cellular extracts from $mHR23B^{+/+}$, $mHR23B^{+/-}$, and $mHR23B^{-/-}$ MEFs using *mHR23B* cDNA as a probe. As a loading control for the amount of RNA, the blot was reprobed with *mHR23A* cDNA (data not shown). (E) Immunoblot analysis of mHR23B protein in cellular extracts from $mHR23B^{+/+}$, $mHR23B^{+/-}$, and $mHR23B^{-/-}$ MEFs using polyclonal antibodies against the human HR23B protein (top blot). Polyclonal antibodies against the human HR23A protein (bottom blot) and the human XPC protein (data not shown) were used as a loading control and to check whether mHR23A protein is expressed in *mHR23B* MEFs. The asterisks indicate aspecific cross-reacting bands.

expression of the *mHR23B* gene was analyzed in MEFs: neither *mHR23B* mRNA nor mHR23B protein could be detected in $mHR23B^{-/-}$ cells by RNA and immunoblot analyses, respectively (Fig. 1D and E). We conclude that we have created *mHR23B* null mutants. Homozygous mouse mutants and cell lines from the two independent ES transformants yielded identical results in all subsequent studies, indicating that the findings reported below are not due to uncontrolled events that might have occurred in one targeted ES clone but are the result of *mHR23B* inactivation.

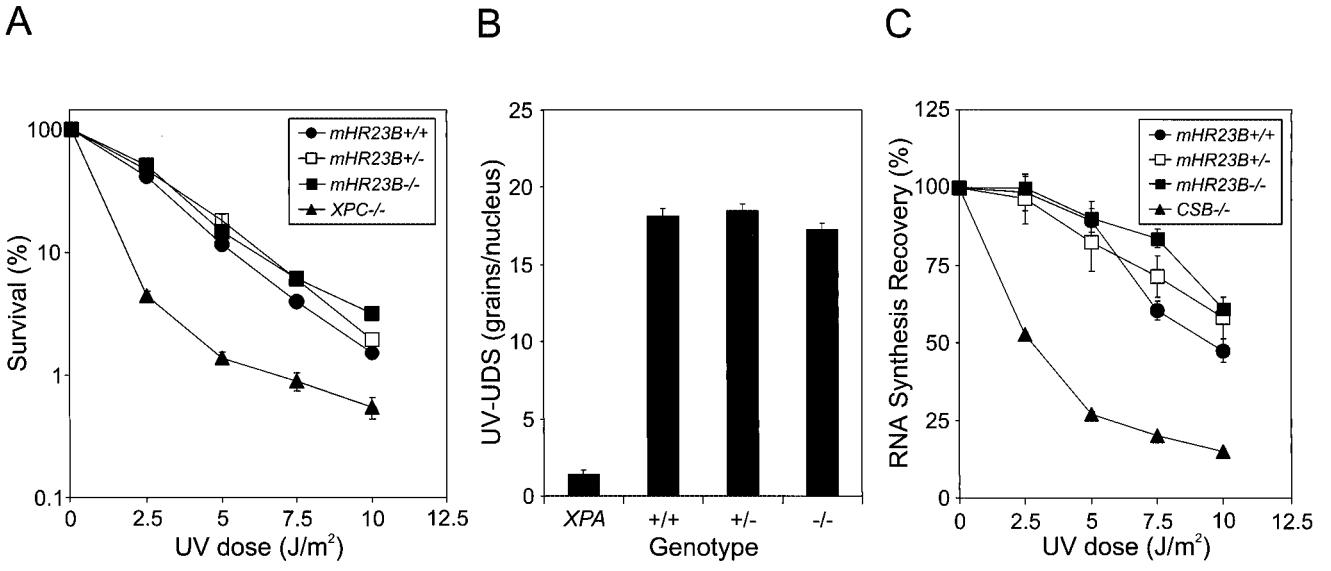

FIG. 2. Repair characteristics of *mHR23B*-deficient MEFs. (A) UV survival curves of $mHR23B^{+/+}$, $mHR23B^{+/-}$, and $mHR23B^{-/-}$ fibroblast lines. Identical results were obtained with three other cell lines of $mHR23B^{+/+}$ and $mHR23B^{+/-}$ and with five other independent lines of $mHR23B^{-/-}$ MEFs (data not shown). $XPC^{-/-}$ fibroblasts were included as a negative control. Cells were exposed to different doses of UV (254-nm wavelength). After 4 or 5 days, the number of proliferating cells was estimated from the amount of radioactivity incorporated during a 3-h pulse with [^{3}H]thymidine. (B) Global genome repair (UDS) in $mHR23B^{+/+}$, $mHR23B^{+/-}$, and $mHR23B^{-/-}$ fibroblast lines. Three other lines of $mHR23B^{+/+}$ and $mHR23B^{+/-}$ and five independent lines of $mHR23B^{-/-}$ were tested with consistent results (data not shown). $XPA^{-/-}$ fibroblasts were included as a negative control. Cells were irradiated with UV (16 J/m^2) (254-nm wavelength) and labeled with [^{3}H]thymidine. Incorporation of radioactivity was measured by autoradiography and counting the grains (average of 50 nuclei per cell line) (the standard errors of the mean are indicated by the error bars). (C) RNA synthesis recovery after UV exposure of $mHR23B^{+/+}$, $mHR23B^{+/-}$, and $mHR23B^{-/-}$ fibroblast lines. Three other lines of $mHR23B^{+/+}$ and $mHR23B^{+/-}$ and five other independent lines of $mHR23B^{-/-}$ were assayed with similar outcome (data not shown). $CSB^{-/-}$ fibroblasts served as a negative control. At 16 h after exposure to different doses of UV (254-nm wavelength), the residual RNA synthesis was measured by scintillation counting following a 1-h pulse-labeling with [^{3}H]uridine. For each genotype, comparable results were obtained by counting the grains after autoradiography (data not shown).

***mHR23B*-deficient cells are NER proficient.** In view of the role of *S. cerevisiae* RAD23 in NER and the tight interaction of mHR23B with XPC (26), we examined cellular survival of wild-type, heterozygous, and homozygous *mHR23B* mutant MEFs after exposure to increasing UV doses. Unexpectedly, UV survival of $mHR23B^{+/-}$ and $mHR23B^{-/-}$ cells appeared indistinguishable from that of the wild-type cells (Fig. 2A). Moreover, *mHR23B*-deficient MEFs show normal DNA repair synthesis (UDS [Fig. 2B]) and recovery of RNA synthesis after UV exposure (Fig. 2C), indicating that neither GG-NER nor TC-NER subpathways were affected. Also, in other respects (e.g., morphology, growth rate, etc.), *mHR23B*-deficient MEFs behaved normally. Assuming that a total *mHR23* inactivation would result in a DNA repair deficiency, as in *S. cerevisiae* (28, 48), these data suggest that mHR23A can fully substitute for mHR23B, at least for its function in NER, not only in vitro but also in vivo.

***mHR23B* deficiency causes impaired embryonic development and intrauterine death.** When (phenotypically normal) heterozygous animals were crossed to produce *mHR23B*-deficient mice, the targeted *mHR23B* allele was found to segregate at a ratio far below that expected by Mendelian inheritance (~10-fold) (a total of 671 animals analyzed) (Table 1), suggesting that a lack of mHR23B protein causes intrauterine and/or perinatal death. Since *mHR23B*-deficient MEF lines were obtained at an almost Mendelian ratio (data not shown), lethal events must occur after day 13.5 of gestation (E13.5). Analysis of a large series of embryos at different stages of development revealed a near twofold reduction in the number of viable *mHR23B*-deficient embryos between E13.5 and E15.5 (Table 1). Since at E18.5, 50% of the *mHR23B*-deficient embryos were still alive (and the litters that were born contained only 10% of the expected numbers of knockout animals), 80% of the remaining embryos are assumed to have died immediately prior to, during, or shortly after birth, which is consistent with the observed high number of dead newborn $mHR23B^{-/-}$ mice.

mHR23B-deficient embryos (E13.5 to E19.5) showed clear signs of growth retardation and were readily recognized by a marked reduction in body size (Fig. 3). This is reflected by a reduced body weight, which becomes more pronounced towards term (data not shown). All $mHR23B^{-/-}$ embryos alive at stages E13.5 to E19.5 appeared pale, whereas major blood

TABLE 1. Intrauterine and perinatal lethality of $mHR23B^{-/-}$ mutants at different embryonic and fetal stages

Stage	No. of mice studied	No. of $mHR23B^{-/-}$ mice		No. of $mHR23B^{-/-}$ mice expected/no. of $mHR23B^{-/-}$ mice observed
		Expected (if Mendelian inheritance)	Observed	
E13.5	70	17.5	14	1.3
E15.5	72	18.0	9	2.0
E18.5	162	40.5	19	2.1
Newborn	671	167.8	16	10.5

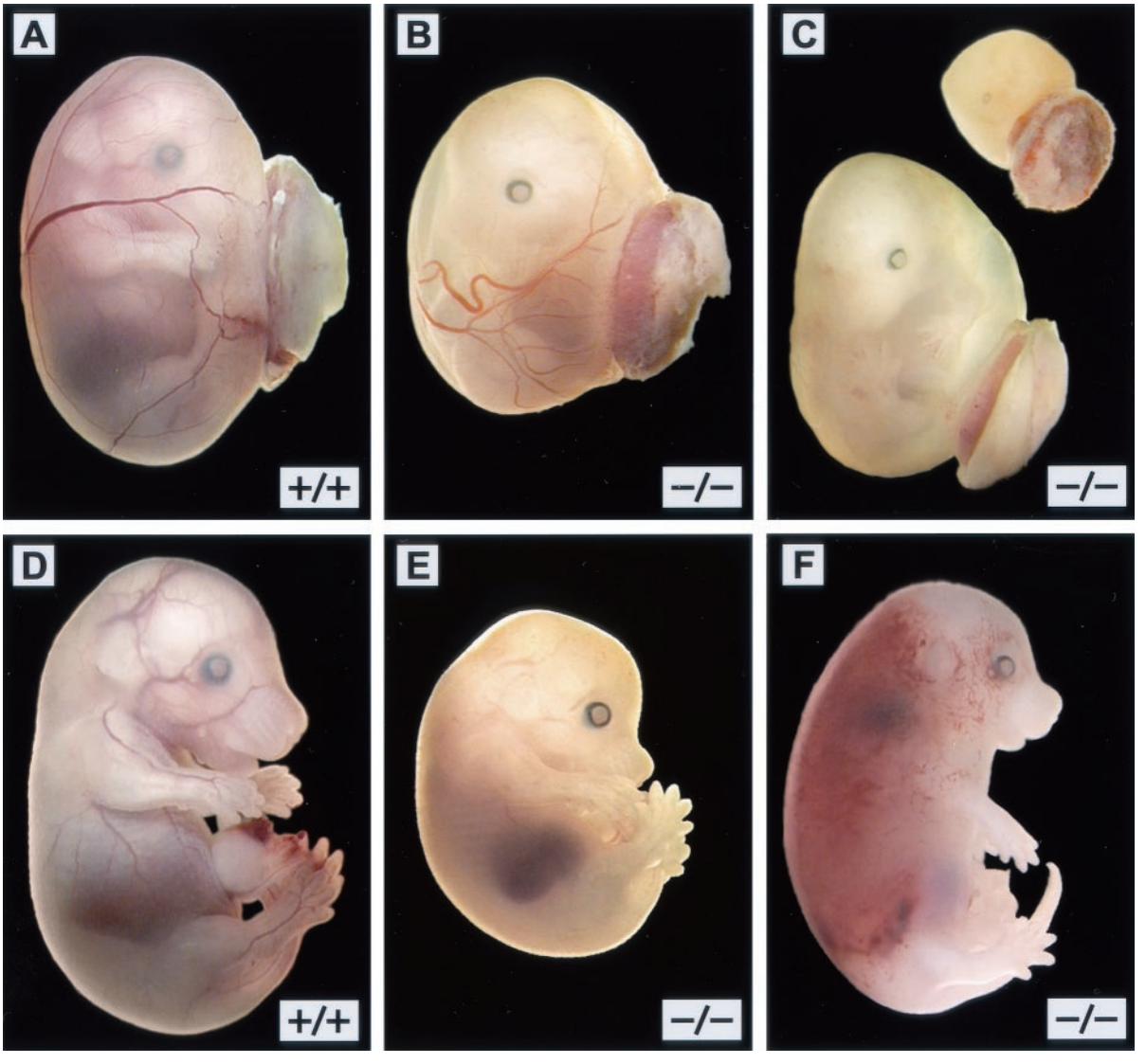

FIG. 3. Developmental impairment in *mHR23B*$^{-/-}$ embryos at E15.5. *mHR23B*$^{+/+}$ (A and D) and *mHR23B*$^{-/-}$ (B, C, E, and F) embryos with (A to C) and without (D to F) amniotic or chorionic plates and placentas. The embryo in panel A is identical to the embryo in panel D, and the embryo in panel B is identical to that in panel E. *mHR23B*$^{-/-}$ embryos display retarded growth and impaired vascularization (B and E), intrauterine death (C), and internal bleeding (F).

vessels were not clearly visible (Fig. 3B and E). This suggests that vascularization and/or blood supply was poor. In addition, large numbers of *mHR23B*$^{-/-}$ embryos showed edema (Fig. 3F). Also, embryos with interstitial bleeding throughout the body were found (Fig. 3F). Moreover, in numerous *mHR23B*$^{-/-}$ embryos (E13.5 to E19.5), the eyelids were not closed and the mouth was widely open, which is a characteristic feature of maceration following embryonic death. Eyelid closure and fusion normally occur between E15.5 and E16.5 of mouse embryonic development. A wide open mouth normally indicates micrognathia or cleft lip resulting from retarded growth of the mandible.

Preliminary histopathological examination of living *mHR23B*-deficient E15.5 and E18.5 embryos revealed no obvious abnormal architecture of vital organs and tissues, and the reduction in organ weight appeared proportional to the reduction in total body weight. However, in one *mHR23B*-deficient E18.5 embryo, we observed an open secondary palate (cleft palate) resulting from imperfect closure of the palatal shelves of the maxilla (in normally developing embryos, this is completed at E16; data not shown). Taken together, these data indicate that the mHR23B protein is required for proper embryonic development and that mHR23A cannot substitute or can substitute only partly for this function.

Inactivation of *mHR23B* causes a placental defect. In line with the pale appearance of a large number of *mHR23B*-deficient embryos, the placentas of *mHR23B*$^{-/-}$ mutants at stage E18.5 ($n = 3$) appeared pale and smaller compared to *mHR23B*$^{+/+}$ and *mHR23B*$^{+/-}$ placentas. Histological examination revealed poor vascularization of mutant placentas, as evident from the reduced number of fetal blood vessels in the labyrinth (Fig. 4A and B). Transmission electron microscopy of

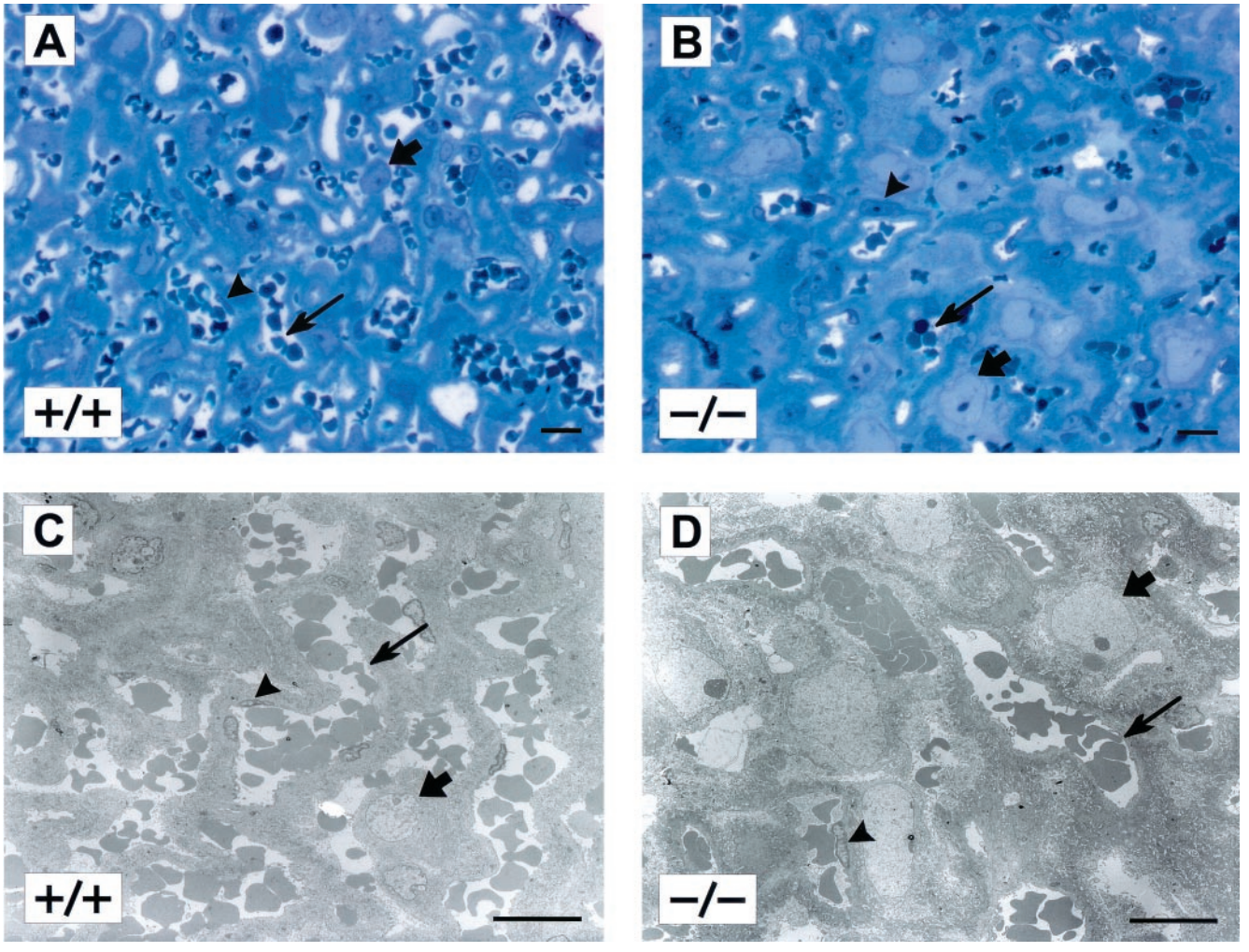

FIG. 4. Placental defect in *mHR23B*$^{-/-}$ embryos at E18.5. Histological 1-μm-thick sections (A and B) and transmission electron micrographs (C and D) of *mHR23B*$^{+/+}$ (A and C) and *mHR23B*$^{-/-}$ (B and D) placentas. *mHR23B*$^{-/-}$ placenta shows swollen trophoblastic cells (small black arrows) and significantly reduced vascularization (blood vessels indicated by large black arrows and endothelial cells indicated by black arrowheads). Additionally, in contrast to normal placental labyrinth of the wild-type mouse placenta, the vascularization and vascular basement membranes in the mutant placenta seem to be disturbed. Scale bars, 10 μm.

mHR23B$^{-/-}$ placentas (n = 3) revealed swollen trophoblastic cells (Fig. 4C and D). In addition, altered morphology of the vascular basement membrane of *mHR23B*$^{-/-}$ placentas was observed (Fig. 4D). The vascular basement membrane of *mHR23B*$^{-/-}$ placentas was darker and thicker than that of wild-type placentas, which might affect the exchange of gases and transport of nutrients and waste products.

***mHR23B*-deficient mice show retarded growth and facial dysmorphology.** Despite the pronounced impact of the *mHR23B* deficiency on embryonic development, about one-tenth of the expected number of homozygous mutant mice was found alive in litters born from heterozygous breeding couples (Table 1). Like *mHR23B*$^{-/-}$ embryos, newborn homozygous mutant mice showed a marked reduction in body size and are readily distinguishable from their heterozygous and wild-type littermates (Fig. 5A). After the mice were weaned, we did not notice any further weight loss of *mHR23B*$^{-/-}$ animals. As evident from body weight measurements, *mHR23B*$^{-/-}$ mice display retarded growth, particularly in the last days before weaning (day 21). Up to 7 weeks after birth, the average body weight of homozygous mutant males (n = 4) and females (n = 2) was still approximately 50% lower than that of wild-type (n = 3) and heterozygous (n = 8) littermates (Fig. 5B). This situation remained throughout life (body weight at 3 months shown in Fig. 5C). Vital organs were proportionally reduced in size (data not shown). Adult *mHR23B*$^{-/-}$ males and females (up to 1 year and older) lacked fatty tissues, while excessive fat was observed in the abdominal cavity of wild-type mice. However, histopathological examination of the vital organs, sciatic nerve, and skeletal muscle from adult *mHR23B*-deficient mice (n = 4) failed to reveal any obvious abnormality (data not shown).

All *mHR23B*-deficient mice and embryonic stages analyzed from E16.5 on showed facial dysmorphology. The nose had a blunted shape rather than the tapered appearance characteristic for rodents due to hypoplasia of the maxilla and mandible (Fig. 5D and E). In addition, more than one-third of the *mHR23B*-deficient mice developed so-called elephant teeth (overgrown teeth). The cause of death at <0.5 to 1 year of age

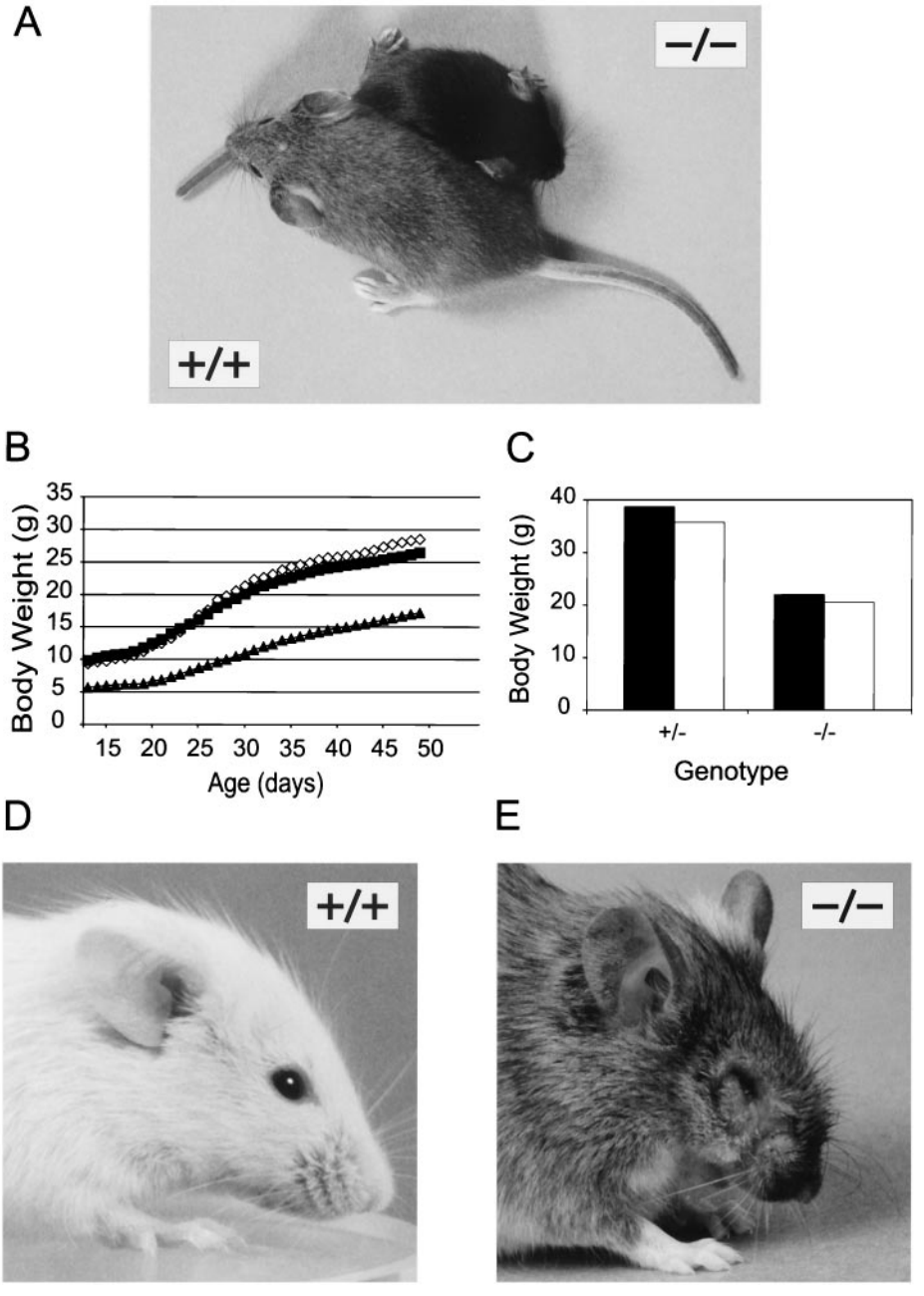

FIG. 5. Growth retardation in *mHR23B*$^{-/-}$ mice. (A) A 19-day-old wild-type male mouse (brown) and its smaller *mHR23B*$^{-/-}$ (black) littermate. (B) Growth curve of *mHR23B* mice. Data for *mHR23B*$^{+/+}$ (n = 3 [males]) (open diamonds), *mHR23B*$^{+/-}$ (n = 8 [5 males and 3 females]) (closed squares), and *mHR23B*$^{-/-}$ (n = 6 [4 males and 2 females]) (closed triangles) are shown. The average body weights (in grams) were monitored for 5 weeks. (C) Average body weights (in grams) of 93-day-old *mHR23B*$^{+/-}$ (n = 8 [5 males and 3 females]) and *mHR23B*$^{-/-}$ (n = 6 [4 males and 2 females]) mice. Data are shown for males (black bars) and females (white bars). (D) Adult *mHR23B*$^{+/+}$ mouse. (E) The eyelids are inflamed in an adult *mHR23B*$^{-/-}$ mouse and are surrounded by a large amount of tears or eye fluid. The head of a *mHR23B*$^{-/-}$ mouse appears irregularly shaped due to hypoplasia of the maxilla and mandible.

may be secondary to the poor overall condition of the mutant mice. However, we did not observe cancer thus far.

***mHR23B*-deficient mice have ocular pathology.** Some 7 to 10 days after birth, *mHR23B*-deficient mice started to develop eye pathology, characterized by excessive eye fluid and swelling of the eyelids. Animals refrained from opening their eyes widely. Probably as a result of the continuously drenched eyes, *mHR23B*-deficient mice showed excessive washing activities. These features persisted into adulthood with frequent signs of inflammation in eyelids (Fig. 5E) that could not be treated by application of eye ointment (Terramycin containing oxytetracycline-polymyxin). In addition, a large number of *mHR23B*-deficient animals seemed to suffer from itching, as evident from extensive scratching, which was not restricted to the head region but also involved the ears and the neck line. Some *mHR23B*-deficient mice had opaque eyes (data not shown).

A

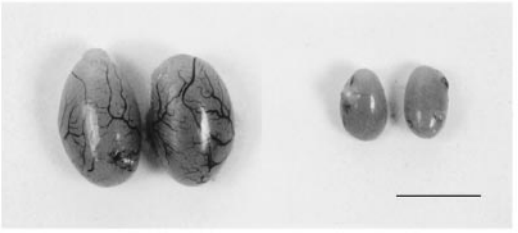

B

Average Weights of Body and Sexual Organs in Wildtype and *mHR23B* Knockout Male Mice

	Wildtype*	Knockout**
Body Weight (g)	37.8	18.5
Testes (mg)	221.1	30.4
Epididymides (mg)	79.6	31.5
Seminal Vesicles (mg)	59.5	35.6

* Consisted of 6 (4.5-month-old) mice (+/+ n=3; +/- n=3)
** Consisted of 6 (4.5-month-old) *mHR23B-/-* mice (n=6)

FIG. 6. The growth of the testes of *mHR23B*$^{-/-}$ males is retarded. (A) Macrograph of adult wild-type (left) and *mHR23B*$^{-/-}$ (right) testes. Besides reduction in size, blood vessels are not clearly visible in *mHR23B*$^{-/-}$ testes. Scale bar, 5 mm. (B) Average weights of body and sexual organs in wild-type and *mHR23B*$^{-/-}$ male mice.

Histological analysis of *mHR23B*-deficient mice ($n = 6$) confirmed that the mice had conjunctivitis. In addition, in the corners of the eyes of *mHR23B*-deficient mice, inflammation cells containing polymorphic nuclei (neutrophils) were observed possibly due to infections (data not shown). A clear cause of the wet eyes was not detected. The tear-producing glands showed no overt abnormalities. However, in one *mHR23B*-deficient mouse, the number of conjunctival goblet cells that produce the mucous layer of the tear film was determined ($n = 2$) and found to be reduced. The drainage of the tears was checked in one *mHR23B*-deficient animal and appeared normal. Moreover, we failed to observe any abnormalities in other parts of the eye, such as the retina (data not shown).

To examine the possibility of any inflammatory disease, the ratio of immunoglobulin A (IgA), IgG, and IgM and the white blood cell counts of adult *mHR23B*-deficient mice ($n = 5$) were determined, but abnormalities were not found, indicating that the immunological system is not compromised (data not shown).

Defective spermatogenesis in *mHR23B*$^{-/-}$ male mice. Attempts to use *mHR23B*$^{-/-}$ males in breeding protocols with either *mHR23B*$^{-/-}$ or wild-type female mice did not result in pregnancies. Since *mHR23B*$^{-/-}$ males show mating activity (as evident from the presence of copulatory plugs in the female mice), their inability to produce progeny appears not to be related to either reduced body size (which may affect physical sexual performance) or hormonal disturbances. Inspection of the reproductive organs of adult *mHR23B*$^{-/-}$ males (3.5 to 7 months of age; $n = 11$) disclosed a disproportionate reduction in the size of the testes (Fig. 6A). Whereas the weight of all internal organs was proportional to the twofold reduction in body weight, the weight of *mHR23B*$^{-/-}$ testes was reduced by about sevenfold. The weight of *mHR23B*$^{-/-}$ epididymides and seminal vesicles was reduced by about twofold (Fig. 6B).

Morphology of seminal vesicles of *mHR23B*-deficient males ($n = 2$) showed no abnormalities. However, histological examination of the testes of *mHR23B*-deficient males revealed seminiferous tubules with a small diameter and relatively abundant interstitial tissue in all animals analyzed ($n = 11$) (Fig. 7). Most striking is the total absence of spermatogenesis, which is in line with the absence of sperm cells in the epididymis (Fig. 7B). In the tubules, Sertoli cells appear to be the predominant cell type (Fig. 7D and F). In the center of most tubules, we observed a concentration of cells, which are typical of Sertoli cell clusters, which represent Sertoli cells detached from the basal membrane of the seminiferous tubule (Fig. 7D and F). Such clusters were not observed in wild-type seminiferous tubules, containing all stages of spermatogenesis (Fig. 7C and E). Release of Sertoli cells from the basal membrane and clustering in the lumen has been observed in other male mouse sterility models, particularly in the older animals (32).

The impairment of spermatogenesis in adult *mHR23B*-deficient mice might reflect a primary defect, resulting in a block at an early or later phase of spermatogenesis. To study this in more detail, a histological analysis was performed on the testes of 15-day-old *mHR23B*$^{-/-}$ animals, when spermatogenesis is normally initiated. Morphology of the testis of a *mHR23B*-deficient mouse revealed no initiation of spermatogenesis compared to normal initiation of spermatogenesis, with presence of pachytene spermatocytes, in the testis of a wild-type mouse. The majority of the tubules of the testis of a 15-day-old *mHR23B*-deficient mouse showed a Sertoli-cell-only phenotype, although a few tubules contained some spermatogonia (Fig. 7G and H). Histological examination of an E15.5 *mHR23B*-deficient male revealed normal urogenital morphology of Müllerian duct regression and Wolffian duct development, indicating testicular production of anti-Müllerian hormone (AMH) by Sertoli cells and testosterone by the interstitial Leydig cells. Although testicular histology of E15.5 *mHR23B*-deficient animals displayed normal Sertoli cells, the number of gonocytes (originating from primordial germ cells) seemed to be reduced compared to the testes of wild-type mice (Fig. 8).

***mHR23B*$^{-/-}$ females exhibit reduced fertility.** In contrast to *mHR23B* homozygous mutant males, *mHR23B*$^{-/-}$ females ($n = 5$) were fertile. However, compared to *mHR23B*$^{+/+}$ or *mHR23B*$^{+/-}$ females, fertility of *mHR23B*-deficient females ($n = 5$) was clearly reduced. Copulatory plugs were found after interbreeding with wild-type or *mHR23B*$^{+/-}$ males, but litters born from *mHR23B*-deficient females were consistently smaller than normal (only one or two pups/litter). Histology of *mHR23B*$^{-/-}$ ovaries ($n = 3$) showed a full spectrum of follicular development including Graafian follicles and corpora lutea, indicating normal endocrine regulation of ovarian function by follicle-stimulating hormone and luteinizing hormone (data not shown).

Additional findings in *mHR23B*$^{-/-}$ mice. A large proportion of *mHR23B*-deficient mice frequently suffered from inflamed or swollen anuses in parallel with ulcers, resulting from rectal prolapse. Also, the mice had soft oily feces, which may point to an intestinal malfunctioning. The skin of *mHR23B*-deficient mice ($n = 16$) appeared thinner than that of wild-type mice.

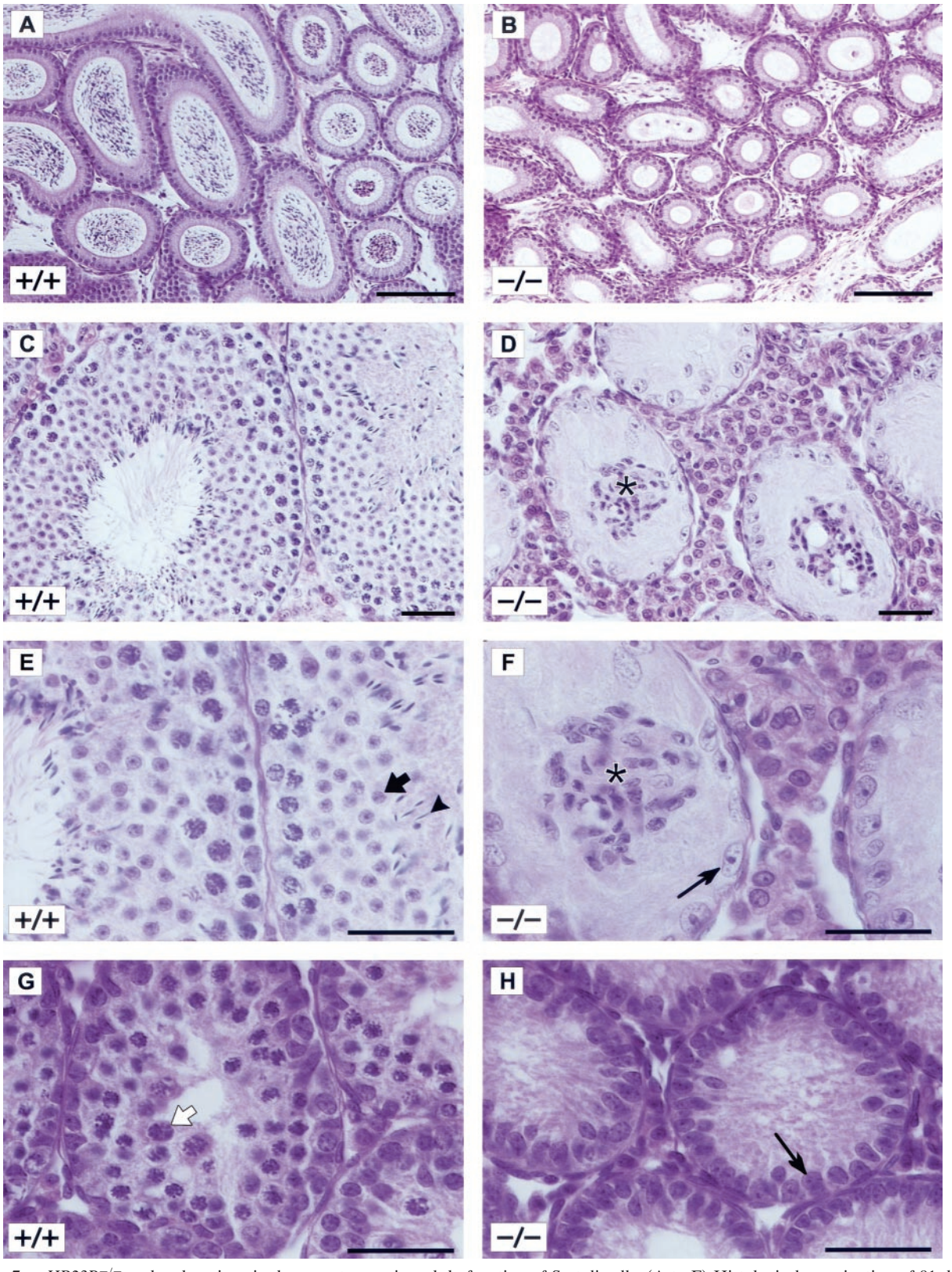

FIG. 7. *mHR23B*$^{-/-}$ males show impaired spermatogenesis and dysfunction of Sertoli cells. (A to F) Histological examination of 91-day-old caput epididymis (A and B) and testis (C to F) from wild-type (A, C, and E) and *mHR23B*$^{-/-}$ mice (B, D, and F). Epididymis of a wild-type mouse (A) is filled with sperm cells, which are absent in the epididymal tubules of *mHR23B*$^{-/-}$ mouse (B). Normal spermatogenesis led to spermatids (small black arrow) and spermatozoa (black arrowhead) shown toward the lumen in wild-type mouse testis (C and E [panel E is a higher-magnification view of the section shown in panel C]). In contrast, spermatogenesis is impaired in *mHR23B*$^{-/-}$ testes (D and F [panel F is a higher-magnification view of the section shown in panel D]). Seminiferous tubules of *mHR23B*$^{-/-}$ testis show Sertoli cell nuclei at the normal position near the basal membrane (black arrow) and Sertoli cell clusters (indicated by asterisks) in the lumen. (G and H) Histological sections of 15-day-old testis from wild-type (G) and *mHR23B*$^{-/-}$ (H) mice. Tubules of *mHR23B*$^{-/-}$ testis show a Sertoli-cell-only phenotype, with predominant appearance of Sertoli cells (black arrow points to Sertoli cell nucleus) compared to wild-type testis, with the presence of spermatocytes (small white arrow). Scale bars, 100 μm.

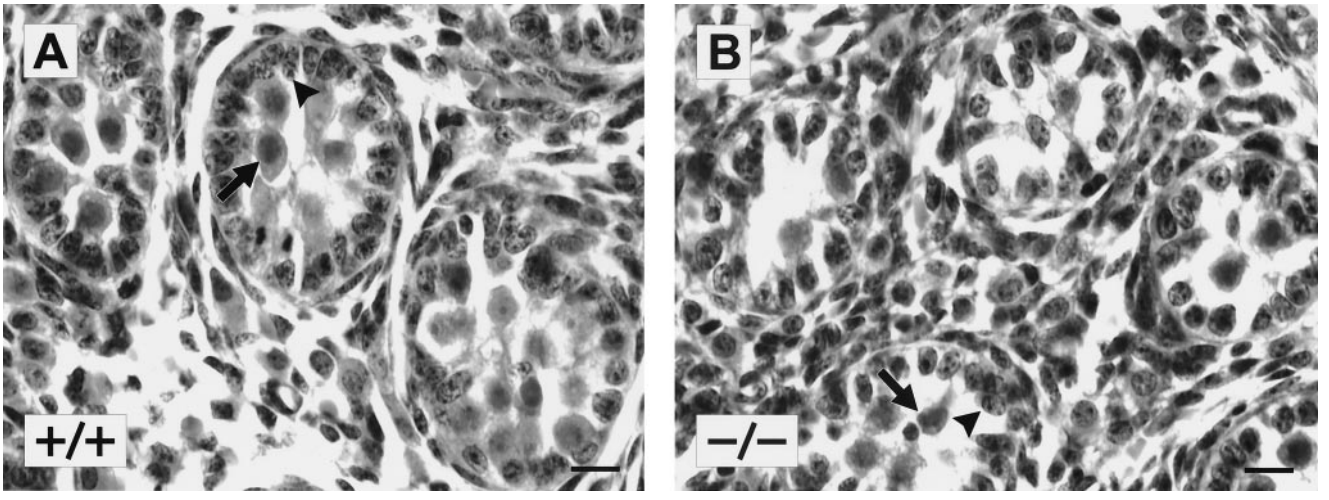

FIG. 8. *mHR23B*$^{-/-}$ embryos at E15.5 show impaired development of gonocytes. Histological analysis of the tubules of E15.5 testis from wild-type (A) and *mHR23B*$^{-/-}$ (B) mutants. Sertoli cell nuclei are indicated by black arrowheads. Compared to wild-type testis, tubules of *mHR23B*$^{-/-}$ testis show less gonocytes (black arrows). Scale bars, 10 μm.

However, the skin of *mHR23B*-deficient mice ($n = 4$) showed no overt abnormalities compared with that of wild-type mice (*mHR23B*$^{+/-}$; $n = 2$). In addition, the amount of subcutaneous fat in *mHR23B*$^{-/-}$ mice was comparable to that of wild-type mice (data not shown). Finally, a few *mHR23B*-deficient mice showed abnormal behavior, like jumping ($n = 3$) and circling or waltzing ($n = 1$), although definite conclusions await analysis using several behavioral tests with a larger number of animals.

DISCUSSION

***mHR23* deficiency does not result in a NER defect.** RAD23 mutants are unique among the *S. cerevisiae* NER mutants in several respects. Despite an intermediate UV sensitivity, suggesting partial NER impairment, deletion mutants of both *S. cerevisiae* and *Schizosaccharomyces pombe* do not display, paradoxically, detectable global genome and transcription-coupled repair, indicating that NER is completely disturbed (24, 46). Within the NER machinery, RAD23 is the only component with multiple connections with the ubiquitin system. The RAD23 protein has a ubiquitin-like N terminus that is essential for its function in repair in vivo (48). The two ubiquitin-associated domains within the protein are very strongly conserved, which underlines their functional importance. The protein interacts physically via its ubiquitin-like domain with components of the 26S proteasome and inhibits multiubiquitination in vitro (33, 35). In view of its strong interaction with RAD4, it is likely that the main role of RAD23 in NER is mediated via this repair component. Remarkably, *S. cerevisiae* RAD4 and RAD23 appear to be involved in both NER subpathways, whereas the mammalian counterpart of RAD4, XPC, is involved only in GG-NER (28, 44). Of the two homologs of RAD23 in mammals, hHR23B is the main partner of XPC (26). The XPC-hHR23B heterodimer is identified as the first initiator of damage recognition in global genome repair, and it is also found to stimulate XPC in in vitro NER (38).

In this study, we have analyzed the function of mHR23B in vivo by generating an *mHR23B* knockout mouse model. Surprisingly, in contrast to *S. cerevisiae*, no apparent NER phenotype is detected in *mHR23B*-deficient cells, which are not UV sensitive and show efficient global genome repair and transcription-coupled repair (Fig. 2). These data demonstrate that NER, and in particular the function of *XPC*, is not significantly affected by the absence of *mHR23B*. Assuming that as in *S. cerevisiae*, the mammalian RAD23 homologs are important for NER, the most plausible interpretation for our findings is that in the absence of mHR23B, the mHR23A protein can functionally replace it, including the binding and stimulation of XPC. This is consistent with the in vitro redundancy between the human HR23 homologs in NER (39) and the recent identification of an XPC-hHR23A subcomplex in whole-cell extracts (1). These findings support an in vivo function of HR23A in GG-NER. Thus, they argue against the model that the HR23A protein specifically interacts with a hitherto unidentified second RAD4-like homolog in mammals specific for TC-NER, so that both together would cover the function of the single RAD4 and RAD23 genes in *S. cerevisiae* (14). However, it remains puzzling why the HR23B protein is normally predominantly associated with XPC in living cells, whereas this study suggests that HR23A appears to be equally able to perform this function in NER (37, 41). Therefore, the functional distinction between HR23A and HR23B proteins is still unresolved.

Mice lacking *mHR23B* display a severe, unexpected phenotype. Whereas an apparent NER defect could not be detected, *mHR23B*-deficient mice exhibit a severe phenotype, which is quite different from the abnormalities observed in mouse models for other NER genes. A complete *mHR23B* deficiency causes impaired embryonic development, poor vascularization, growth retardation, male sterility, and facial dysmorphology (Table 2). In contrast, inactivation of the mammalian *XPC* gene, the other component of the XPC-mHR23B complex, results in a GG-NER defect which is accompanied only by UV sensitivity and UV-induced skin cancer predisposition (4, 34). Even a total NER defect as demonstrated by *XPA*-deficient

TABLE 2. Summary of phenotypical analysis of *mHR23B*$^{-/-}$ mice

Phenotypic trait	No. of mice affected/ no. of mice screened
Reduced body weight	16/16
Eye pathology	16/16
Fertility	
Sterility in males	11/11
Reduced fertility in females	5/5
Facial dysmorphology	
Elephant teeth	>6/16
Shape of the face (maxilla or mandible)	16/16
Other findings	
Thin skin	16/16
Rectal prolapse	>5/16
Itching or washing	>3/16
Circling (waltzing)	1/16
Six toes on a foot	1/16

mice allows apparently normal development and life span (11, 29).

Mutations in several NER factors can give rise to a spectrum of additional features that at first glance seem not to be associated with a NER defect. For example, patients with CS show a combination of sun sensitivity, short stature, severe neurological abnormalities, and a characteristic bird-like facies, and TTD patients also have ichthyosis and many symptoms of CS (3, 7). These symptoms are explained by the fact that the corresponding proteins have additional functions outside the NER context, particularly transcription. For instance, in the case of the *CSA* and *CSB* mutants, sensitivity of the transcription process to a wider range of lesions hampering transcription may contribute to the severe developmental and neurological complications and premature ageing of CS patients. Similarly, the engagement of dual XPB and XPD helicases of TFIIH in both NER and basal transcription initiation may give rise to the typical TTD symptoms (8). However, the CS and TTD symptoms are quite distinct from the abnormalities exhibited by the *mHR23B* mouse mutant. A condition with a superficial resemblance to the phenotype of *mHR23B* deficiency is cerebro-oculo-facio-skeletal (COFS) syndrome which is considered within the same differential diagnosis as CS (15). COFS is a rare birth defect disorder with an autosomal recessive inheritance characterized by progressive brain and eye defects leading to skeletal and craniofacial abnormalities, postnatal growth deficiency, genital hypoplasia, and early death. It should be kept in mind that such comparisons can be quite misleading, and further research will be required to determine whether mHR23B is implicated in some form of this disease or in other human disorders. Our work demonstrates that *mHR23B* is essential for normal development of the mouse and implies an additional function besides its role in GG-NER, which is not compensated or only partially compensated for by mHR23A.

***mHR23B* is essential for growth and development.** The phenotypic abnormalities detected during the intrauterine development of *mHR23B*-deficient mice included prenatal (or early postnatal) death, disturbed growth, as well as abnormalities involving improper differentiation of the vascular basement membrane in the placental labyrinth and vascularization. The placenta is essential for embryonic survival beyond E11.5, as it forms vascular connections necessary for maternal-fetal exchange of gases, nutrients, and waste products (6). Thus, the transport of nutrients to the embryo may be limited in the damaged labyrinth region of homozygous mutant embryos. This may explain a number of abnormal features, such as early embryonic death, swollen trophoblast cells, small placenta, and poor, delayed development resulting in smaller embryos. The growth of *mHR23B*$^{-/-}$ embryos that live beyond E11.5 appears to be retarded. We speculate that these embryos have a placenta with sufficient function to allow survival to term but not normal growth and development. This may also explain the reduction in weight.

***mHR23B* deficiency is related to an ocular defect and facial dysmorphology.** Mice lacking mHR23B function exhibit wet eyes and inflammation of the eyelids and conjunctiva. We found no gross abnormalities in the tear-producing tissues, and drainage of tears also appeared normal. However, the reduction of conjunctival goblet cells that was apparent in one of the examined eyes may point to an involvement of vitamin A in this phenotype. Vitamin A is necessary for proper differentiation and maintenance of the mucosal epithelium. Lack of vitamin A causes a depletion of goblet cells, which alters the composition of the tear film and eventually can lead to xerosis and inflammation of the eye (22). *mHR23B*-deficient mice may suffer from vitamin A deficiency in conjunction with disturbed lipid resorption. This would fit with other observations found for *mHR23B*-deficient mice, such as reduced body weight, low amount of body fat, and soft, oily feces (probably due to rectal prolapse with an unknown cause).

mHR23B-deficient mice also display abnormalities of facial and tooth development. It is possible that the biting or chewing process is disturbed because of an imperfect positioning of the dental elements in the maxilla and mandible. The facial abnormalities may be a direct result of subtle developmental defects in the head region. However, reduced growth of the palatal shelves is found in one *mHR23B*$^{-/-}$ embryo. Since the closure of the palate is of critical importance for proper food intake and respiration, this could relate to the death of many *mHR23B*-deficient animals around birth. Therefore, a more systematic analysis of this feature to assess the biological significance of this observation is warranted.

***mHR23B* is associated with male sterility.** Disruption of *mHR23B* causes defective spermatogenesis, resulting in the absence of developing germ cells and a phenotype like that the Sertoli cell-only syndrome. *mHR23A* and *mHR23B* are expressed in all mouse tissues and organs, but both genes show enhanced mRNA levels in testis (42), suggesting that loss of the encoded proteins may have specific gonadal consequences. At E15.5, the tubules contain Sertoli cells with a normal histological appearance. The fetal Sertoli cells have produced AMH, as evidenced by Müllerian duct regression. However, the number of gonocytes seemed somewhat reduced. At day 15 after birth, no initiation of spermatogenesis had taken place and many Sertoli cells had become detached from the basal membrane. The results indicate that failure of spermatogenesis in *mHR23B*$^{-/-}$ animals mainly occurs between E15.5 and day 15 after birth. The action of mHR23B may be involved in development of a normal population of gonocytes, which is capable to support initiation of spermatogenesis. In addition, or alternatively, mHR23B may be required for the postnatal initiation phase of spermatogenesis.

It is not clear why *mHR23B*$^{-/-}$ females show decreased

fertility, while ovarian histology is normal. The reduced fertility of *mHR23B*$^{-/-}$ females may result in part from the growth retardation.

Other functional involvements of mHR23 proteins outside NER may link to the ubiquitin proteolytic pathway. Interestingly, the developmental abnormalities detected in *mHR23B*$^{-/-}$ animals are absent in XPC and other NER-deficient mouse mutants. This strongly suggests that mHR23B has a separate important function, which may involve the ubiquitin/proteasome pathway and which cannot be taken over by mHR23A. In fact, studies in *S. cerevisiae* and mammals have shown that RAD23 associates with the 26S proteasome and that hHR23 proteins play a role in cell cycle regulation (20, 23, 35). In addition, the function of the two UBA domains in the RAD23 homologs is not known, though they are present in different classes of enzymes involved in ubiquitin-dependent proteolysis (21).

The ubiquitin system is essential in all cells and is involved in modification of protein conformation and in degradation of proteins. Numerous proteins are regulated through ubiquitination and therefore inhibition of the ubiquitin system frequently results in a rapid dysregulation of multiple cellular processes and subsequently in apoptosis. The effect of a partial inhibition of ubiquitination is dependent upon the cell type: although lethal to some cells, it is less critical to others. Knockout mouse models with a gametogenic failure suggest that the ubiquitination machinery is important in gametogenesis (2, 13). During spermatogenesis, dramatic changes in protein composition take place, which will require extensive use of the ubiquitin/proteasome machinery. Different phases of mammalian spermatogenesis probably require different specialized activities of the ubiquitin system (2). Mouse models in which genes encoding ubiquitination proteins are mutated result in placental defect, embryonic lethality, abnormal facies, cleft palate, and scratching behavior (18, 30, 31).

Taken together, our data suggest that the mammalian HR23 proteins have a broader function outside NER. To provide further evidence, we are currently generating single knockout *HR23A* mice and cells.

ACKNOWLEDGMENTS

We thank C. Vermeij-Keers for helpful discussions on *mHR23B* mutant embryos and R. Hendriks for enzyme-linked immunosorbent assay and fluorescence-activated cell sorter experiments.

This work was partially supported by The Netherlands Organization for Scientific Research (NWO) (grant SIR 15-2777 and grant TF004 for Diseases of the Elderly), NIH (grant AG17242-02), KWF (EUR 98-1774), and the Dutch Foundation "Vereniging Trustfonds Erasmus Universiteit Rotterdam." This work was also supported by grants from the Ministry of Education, Culture, Sports, Science and Technology of Japan and by the Biodesign Research Program and the Bioarchitect Research Project from RIKEN.

REFERENCES

1. **Araki, M., C. Masutani, M. Takemura, A. Uchida, K. Sugasawa, J. Kondoh, Y. Ohkuma, and F. Hanaoka.** 2001. Centrosome protein centrin 2/caltractin 1 is part of the xeroderma pigmentosum group C complex that initiates global genome nucleotide excision repair. J. Biol. Chem. **276:**18665–18672.
2. **Baarends, W. M., R. van der Laan, and J. A. Grootegoed.** 2000. Specific aspects of the ubiquitin system in spermatogenesis. J. Endocrinol. Investig. **23:**597–604.
3. **Bootsma, D., K. H. Kraemer, J. E. Cleaver, and J. H. J. Hoeijmakers.** 2001. Nucleotide excision repair syndromes: xeroderma pigmentosum, Cockayne syndrome, and trichothiodystrophy, p. 677–703. *In* C. R. Scriver, A. L. Beaudet, W. S. Sly, D. Valle, B. Vogelstein, and K. W. Kinzler (ed.), The metabolic and molecular bases of inherited disease, vol. 1. McGraw-Hill Book Co., New York, N.Y.
4. **Cheo, D. L., L. B. Meira, R. E. Hammer, D. K. Burns, A. T. Doughty, and E. C. Friedberg.** 1996. Synergistic interactions between *XPC* and *p53* mutations in double-mutant mice: neural tube abnormalities and accelerated UV radiation-induced skin cancer. Curr. Biol. **6:**1691–1694.
5. **Chomczynski, P., and N. Sacchi.** 1987. Single-step method of RNA isolation by acid guanidinium thiocyanate-phenol-chloroform extraction. Anal. Biochem. **162:**156–159.
6. **Cross, J. C., Z. Werb, and S. J. Fisher.** 1994. Implantation and the placenta: key pieces of the development puzzle. Science **266:**1508–1518.
7. **de Boer, J., and J. H. J. Hoeijmakers.** 2000. Nucleotide excision repair and human syndromes. Carcinogenesis **21:**453–460.
8. **de Boer, J., H. van Steeg, R. J. Berg, J. Garssen, J. de Wit, C. T. van Oostrum, R. B. Beems, G. T. van der Horst, C. F. van Kreijl, F. R. de Gruijl, D. Bootsma, J. H. J. Hoeijmakers, and G. Weeda.** 1999. Mouse model for the DNA repair/basal transcription disorder trichothiodystrophy reveals cancer predisposition. Cancer Res. **59:**3489–3494.
9. **de Bruijn, W. C.** 1973. Glycogen, its chemistry and morphologic appearance in the electron microscope. I. A modified OsO_4 fixative which selectively contrasts glycogen. J. Ultrastruct. Res. **42:**29–50.
10. **de Laat, W. L., N. G. Jaspers, and J. H. J. Hoeijmakers.** 1999. Molecular mechanism of nucleotide excision repair. Genes Dev. **13:**768–785.
11. **de Vries, A., C. T. van Oostrom, F. M. Hofhuis, P. M. Dortant, R. J. Berg, F. R. de Gruijl, P. W. Wester, C. F. van Kreijl, P. J. Capel, H. van Steeg, et al.** 1995. Increased susceptibility to ultraviolet-B and carcinogens of mice lacking the DNA excision repair gene *XPA*. Nature **377:**169–173.
12. **Friedberg, E. C., G. C. Walker, and W. Siede.** 1995. DNA repair and mutagenesis. ASM Press, Washington, D.C.
13. **Grootegoed, J. A., W. M. Baarends, H. P. Roest, and J. H. Hoeijmakers.** 1998. Knockout mouse model and gametogenic failure. Mol. Cell. Endocrinol. **145:**161–166.
14. **Guzder, S. N., P. Sung, L. Prakash, and S. Prakash.** 1998. Affinity of yeast nucleotide excision repair factor 2, consisting of the Rad4 and Rad23 proteins, for ultraviolet damaged DNA. J. Biol. Chem. **273:**31541–31546.
15. **Hamel, B. C., A. Raams, A. R. Schuitema-Dijkstra, P. Simons, I. van der Burgt, N. G. Jaspers, and W. J. Kleijer.** 1996. Xeroderma pigmentosum-Cockayne syndrome complex: a further case. J. Med. Genet. **33:**607–610.
16. **Hanawalt, P. C.** 2000. DNA repair. The bases for Cockayne syndrome. Nature **405:**415–416.
17. **Hanawalt, P. C., B. A. Donahue, and K. S. Sweder.** 1994. Repair and transcription. Collision or collusion? Curr. Biol. **4:**518–521.
18. **Harbers, K., U. Muller, A. Grams, E. Li, R. Jaenisch, and T. Franz.** 1996. Provirus integration into a gene encoding a ubiquitin-conjugating enzyme results in a placental defect and embryonic lethality. Proc. Natl. Acad. Sci. USA **93:**12412–12417.
19. **Heard, J. M., P. Herbomel, M. O. Ott, A. Mottura-Rollier, M. Weiss, and M. Yaniv.** 1987. Determinants of rat albumin promoter tissue specificity analyzed by an improved transient expression system. Mol. Cell. Biol. **7:**2425–2434.
20. **Hiyama, H., M. Yokoi, C. Masutani, K. Sugasawa, T. Maekawa, K. Tanaka, J. H. J. Hoeijmakers, and F. Hanaoka.** 1999. Interaction of hHR23 with s5a. The ubiquitin-like domain of hhr23 mediates interaction with s5a subunit of 26s proteasome. J. Biol. Chem. **274:**28019–28025.
21. **Hofmann, K., and P. Bucher.** 1996. The UBA domain: a sequence motif present in multiple enzyme classes of the ubiquitination pathway. Trends Biochem. Sci. **21:**172–173.
22. **Huang, A. J., S. C. Tseng, and K. R. Kenyon.** 1991. Change of paracellular permeability of ocular surface epithelium by vitamin A deficiency. Invest. Ophthalmol. Vis. Sci. **32:**633–639.
23. **Kumar, S., A. L. Talis, and P. M. Howley.** 1999. Identification of HHR23A as a substrate for E6-associated protein-mediated ubiquitination. J. Biol. Chem. **274:**18785–18792.
24. **Lombaerts, M., J. I. Goeloe, H. den Dulk, J. A. Brandsma, and J. Brouwer.** 2000. Identification and characterization of the *rhp23(+)* DNA repair gene in *Schizosaccharomyces pombe*. Biochem. Biophys. Res. Commun. **268:**210–215.
25. **Masutani, C., M. Araki, K. Sugasawa, P. J. van der Spek, A. Yamada, A. Uchida, T. Maekawa, D. Bootsma, J. H. J. Hoeijmakers, and F. Hanaoka.** 1997. Identification and characterization of XPC-binding domain of hHR23B. Mol. Cell. Biol. **17:**6915–6923.
26. **Masutani, C., K. Sugasawa, J. Yanagisawa, T. Sonoyama, M. Ui, T. Enomoto, K. Takio, K. Tanaka, P. J. van der Spek, D. Bootsma, et al.** 1994. Purification and cloning of a nucleotide excision repair complex involving the xeroderma pigmentosum group C protein and a human homologue of yeast RAD23. EMBO J. **13:**1831–1843.
27. **Mayne, L. V., and A. R. Lehmann.** 1982. Failure of RNA synthesis to recover after UV irradiation: an early defect in cells from individuals with Cockayne's syndrome and xeroderma pigmentosum. Cancer Res. **42:**1473–1478.
28. **Mueller, J. P., and M. J. Smerdon.** 1996. Rad23 is required for transcription-

coupled repair and efficient overall repair in *Saccharomyces cerevisiae*. Mol. Cell. Biol. **16:**2361–2368.
29. **Nakane, H., S. Takeuchi, S. Yuba, M. Saijo, Y. Nakatsu, H. Murai, Y. Nakatsuru, T. Ishikawa, S. Hirota, Y. Kitamura, et al.** 1995. High incidence of ultraviolet-B or chemical-carcinogen-induced skin tumours in mice lacking the xeroderma pigmentosum group A gene. Nature **377:**165–168.
30. **Perry, W. L., C. M. Hustad, D. A. Swing, T. N. O'Sullivan, N. A. Jenkins, and N. G. Copeland.** 1998. The itchy locus encodes a novel ubiquitin protein ligase that is disrupted in a *18H* mice. Nat. Genet. **18:**143–146.
31. **Pizzuti, A., G. Novelli, A. Ratti, F. Amati, A. Mari, G. Calabrese, S. Nicolis, V. Silani, B. Marino, G. Scarlato, S. Ottolenghi, and B. Dallapiccola.** 1997. *UFD1L*, a developmentally expressed ubiquitination gene, is deleted in CATCH 22 syndrome. Hum. Mol. Genet. **6:**259–265.
32. **Russell, L. D., L. R. Franca, and R. L. Brinster.** 1996. Ultrastructural observations of spermatogenesis in mice resulting from transplantation of mouse spermatogonia. J. Androl. **17:**603–614.
33. **Russell, S. J., S. H. Reed, W. Huang, E. C. Friedberg, and S. A. Johnston.** 1999. The 19S regulatory complex of the proteasome functions independently of proteolysis in nucleotide excision repair. Mol. Cell **3:**687–695.
34. **Sands, A. T., A. Abuin, A. Sanchez, C. J. Conti, and A. Bradley.** 1995. High susceptibility to ultraviolet-induced carcinogenesis in mice lacking *XPC*. Nature **377:**162–165.
35. **Schauber, C., L. Chen, P. Tongaonkar, I. Vega, D. Lambertson, W. Potts, and K. Madura.** 1998. Rad23 links DNA repair to the ubiquitin/proteasome pathway. Nature **391:**715–718.
36. **Sijbers, A. M., W. L. de Laat, R. R. Ariza, M. Biggerstaff, Y. F. Wei, J. G. Moggs, K. C. Carter, B. K. Shell, E. Evans, M. C. de Jong, S. Rademakers, J. de Rooij, N. G. Jaspers, J. H. J. Hoeijmakers, and R. D. Wood.** 1996. Xeroderma pigmentosum group F caused by a defect in a structure-specific DNA repair endonuclease. Cell **86:**811–822.
37. **Sugasawa, K., C. Masutani, A. Uchida, T. Maekawa, P. J. van der Spek, D. Bootsma, J. H. J. Hoeijmakers, and F. Hanaoka.** 1996. HHR23B, a human Rad23 homolog, stimulates XPC protein in nucleotide excision repair in vitro. Mol. Cell. Biol. **16:**4852–4861.
38. **Sugasawa, K., J. M. Y. Ng, C. Masutani, S. Iwai, P. J. van der Spek, A. P. Eker, F. Hanaoka, D. Bootsma, and J. H. J. Hoeijmakers.** 1998. Xeroderma pigmentosum group C protein complex is the initiator of global genome nucleotide excision repair. Mol. Cell **2:**223–232.
39. **Sugasawa, K., J. M. Y. Ng, C. Masutani, T. Maekawa, A. Uchida, P. J. van der Spek, A. P. Eker, S. Rademakers, C. Visser, A. Aboussekhra, R. D. Wood, F. Hanaoka, D. Bootsma, and J. H. J. Hoeijmakers.** 1997. Two human homologs of Rad23 are functionally interchangeable in complex formation and stimulation of XPC repair activity. Mol. Cell. Biol. **17:**6924–6931.
40. **van der Horst, G. T., H. van Steeg, R. J. Berg, A. J. van Gool, J. de Wit, G. Weeda, H. Morreau, R. B. Beems, C. F. van Kreijl, F. R. de Gruijl, D. Bootsma, and J. H. J. Hoeijmakers.** 1997. Defective transcription-coupled repair in Cockayne syndrome B mice is associated with skin cancer predisposition. Cell **89:**425–435.
41. **van der Spek, P. J., A. Eker, S. Rademakers, C. Visser, K. Sugasawa, C. Masutani, F. Hanaoka, D. Bootsma, and J. H. J. Hoeijmakers.** 1996. XPC and human homologs of RAD23: intracellular localization and relationship to other nucleotide excision repair complexes. Nucleic Acids Res. **24:**2551–2559.
42. **van der Spek, P. J., C. E. Visser, F. Hanaoka, B. Smit, A. Hagemeijer, D. Bootsma, and J. H. J. Hoeijmakers.** 1996. Cloning, comparative mapping, and RNA expression of the mouse homologues of the *Saccharomyces cerevisiae* nucleotide excision repair gene *RAD23*. Genomics **31:**20–27.
43. **van Hoffen, A., J. Venema, R. Meschini, A. A. van Zeeland, and L. H. Mullenders.** 1995. Transcription-coupled repair removes both cyclobutane pyrimidine dimers and 6–4 photoproducts with equal efficiency and in a sequential way from transcribed DNA in xeroderma pigmentosum group C fibroblasts. EMBO J. **14:**360–367.
44. **Venema, J., A. van Hoffen, V. Karcagi, A. T. Natarajan, A. A. van Zeeland, and L. H. Mullenders.** 1991. Xeroderma pigmentosum complementation group C cells remove pyrimidine dimers selectively from the transcribed strand of active genes. Mol. Cell. Biol. **11:**4128–4134.
45. **Venema, J., A. van Hoffen, A. T. Natarajan, A. A. van Zeeland, and L. H. Mullenders.** 1990. The residual repair capacity of xeroderma pigmentosum complementation group C fibroblasts is highly specific for transcriptionally active DNA. Nucleic Acids Res. **18:**443–448.
46. **Verhage, R. A., A. M. Zeeman, M. Lombaerts, P. van de Putte, and J. Brouwer.** 1996. Analysis of gene- and strand-specific repair in the moderately UV-sensitive *Saccharomyces cerevisiae rad23* mutant. Mutat. Res. **362:**155–165.
47. **Vermeulen, W., R. J. Scott, S. Rodgers, H. J. Muller, J. Cole, C. F. Arlett, W. J. Kleijer, D. Bootsma, J. H. J. Hoeijmakers, and G. Weeda.** 1994. Clinical heterogeneity within xeroderma pigmentosum associated with mutations in the DNA repair and transcription gene *ERCC3*. Am. J. Hum. Genet. **54:**191–200.
48. **Watkins, J. F., P. Sung, L. Prakash, and S. Prakash.** 1993. The *Saccharomyces cerevisiae* DNA repair gene *RAD23* encodes a nuclear protein containing a ubiquitin-like domain required for biological function. Mol. Cell. Biol. **13:**7757–7765.
49. **Wood, R. D.** 1996. DNA repair in eukaryotes. Annu. Rev. Biochem. **65:**135–167.
50. **Yokoi, M., C. Masutani, T. Maekawa, K. Sugasawa, Y. Ohkuma, and F. Hanaoka.** 2000. The xeroderma pigmentosum group C protein complex XPC-HR23B plays an important role in the recruitment of transcription factor IIH to damaged DNA. J. Biol. Chem. **275:**9870–9875.